Measurement of the Nucleation and Growth Kinetics of Some Middle Distillate Fuels and Their Blends with a Model Biodiesel Fuel

Fatima L. Mota, Sébastien Teychené, Béatrice Biscans

Measurement of the nucleation and growth kinetics of some middle distillates fuels and their blends with a model biodiesel fuel

F.L. Mota[*a], *S. Teychéne*[a], *B. Biscans*[a]

[a] Laboratoire de Génie Chimique UMR 5503 , Université de Toulouse, CNRS Toulouse, France

Abstract

The nucleation kinetics and crystal growth rates of both middle distillates and their blends with a model biodiesel were determined. Being middle distillates complex mixtures of hydrocarbons, a strategy was taken to define the solute and solvent. Different mixtures were prepared from different fuels, and a mixture law was used to calculate the mass percentages of each n-paraffin in the mixture: the difference between experimental and estimated compositions is negligible. An experimental device was set-up to obtain the solubility curve of a distillate, for the first time. The application of the classical homogeneous nucleation theory and the Nývlt's semi-empirical approach allowed to obtain the nucleation rate, interfacial tension and nucleation order. The presence of esters does not have an influence on the solubility curve slope, but they have higher kinetic parameters, and an influence on the interfacial tension. The values found using the Nývlt law are typical for organic systems.

Images were taken as a function of temperature and time, using thermomicroscopy, and image analysis enabled to obtain the crystal growth rates. The mixtures containing esters have in general higher growth rates. The solvent nature plays an important role in the growth, since the other alternative fuels studied have considerably higher growth rates.

* fatima.lisboamota@ensiacet.fr; Phone: (+33)534323604; Fax: (+33)534323700

Keywords: nucleation, growth, kinetics, middle distillates, solubility

1. Introduction

During the distillation of crude oil, the cuts from 180° to 360°C provide the so-called middle distillates, which correspond to complex mixtures of hydrocarbon components including saturates, aromatics, resins and asphaltenes. Middle distillates include diesel, heating fuel (FOD) and jet fuel. Even if the characteristics of FOD and diesel are very similar, there are some non-negligible differences: the FOD has higher nucleation temperatures, what can cause filter clogging in case of use in diesel engines; the viscosity of FOD is significantly higher, what can cause problems in the fuel injection system; the final boiling point of FOD is higher, leading to the formation of deposits; the sulfur content in FOD is limited to 2000 ppm; the cetane number of FOD is significantly lower.[1] So, it is not recommended to use the FOD as an alternative to diesel, even if there is a higher tax rate of diesel than home heating oil. Nevertheless, it is still important to compare their behavior and characteristics.

The high price of crude oils and the worldwide concern for CO_2 emissions support the production and the use of biofuels, in addition to being chemically less complex than the conventional diesels. The final price of biodiesel and its properties depend upon the fats and oils used in its production. Fatty acid methyl esters (FAME) of lipids such as soybean, rapeseed, canola oils, used cooking oil, waste greases or tallow are the most common used.[2] Biodiesel from cheap vegetable oils, such as palm oil, with a large concentration of saturated fatty acid esters has a worst performance at low temperatures having tendency to crystallize, even if it is less vulnerable to oxidation and displays better combustion properties.[3] A biodiesel has in general higher melting point than a conventional diesel, because it is essentially determined by the amount of saturated esters (which have higher melting points) and does not depend upon the composition of the unsaturated esters (which act essentially as solvent). The presence of crystals

in the biodiesel, like in conventional diesels, affects its viscosity, flowability and filterability.[4] Solutions have been proposed in order to overcome the problems with fatty acid esters at low temperatures: the preferred and most widely used is blending biodiesel with conventional diesels. Conventional fuels in blends act as a solvent of precipitated crystals at low temperature which is reflected in improved low temperature properties.[5]

As the temperature decreases, the solubility limit of a middle distillate may be reached and the solution will no longer be able to support all the n-paraffins. The solubility limit of the heaviest n-paraffin components is commonly referred as the cloud point (CP), also known as wax appearance temperature (WAT), and it allows to differentiate between products in terms of performance. The problem of crystallization based on flow conditions, pressure and temperature, is transverse to all activities in the oil industry with major economic consequences: production, transportation, refining, formulation of finished products, and the use of fuels. However, deviations from the expected crystallization behaviour may occur caused by the presence of other components in the crystal growth medium. These components, such as aromatics, asphaltenes, resins, water, additives, and shorter chained n-paraffins, can impact a number of factors: crystal morphology, crystal growth rate, nucleation kinetics, crystallization thermodynamics, and dissolution kinetics.[6]

Solid formation, impossible at lower concentration than that of the solubility onset at the given temperature and pressure conditions, may take place at a concentration higher than the theoretical solubility level. The difference between the actual value of the solute concentration at the crystallization operating point and the theoretical solubility onset is called supersaturation (S), and is a fundamental factor in crystallization dynamics. Supersaturation is the driving force for both the initial nucleation step and the following crystal growth.

The ideal zone for the crystal growth is the metastable zone localized between the solubility and supersaturation curves. The metastable zone width (MSZW) is of major importance in crystallization and depends on: saturation temperature, solvent, impurities or seeds, stirring and cooling rate. Once the MSZW is determined, it is possible to carry out a crystallization process where a constant supersaturation is maintained throughout the cooling, leading to nearly constant nucleation and crystal growth rate.[7] The polythermal technique is one of the most widely used for determining the MSZW: it involves cooling a solution at a fixed rate until nucleation, and the process is repeated for a variety of rates. Thermal methods are very convenient to evaluate the onset of nucleation or complete dissolution of crystals, and also to provide information about their kinetics. The detection method used has a great influence on the kinetics since there is a time lag between nucleation and a detectable crystal size. The structure of the critical nucleus for a given supersaturation is theoretically impossible to establish and the extent of nuclei growing beyond the critical size previous to detection may strongly depend on the selected method.

Saturation temperatures and MSZW were measured for the n-paraffins C_{18} to C_{29} and for binary mixtures of C_{20} and C_{22} crystallized from n-dodecane and m-xylene solvents by Gerson et al.[8] The MSZW obtained illustrates the effect of growth environment on the crystallization process. The nucleation kinetics data obtained from induction time measurements show the effect of increasing solute concentration on critical cluster size together with the value of interfacial tension.[8]

The main objective of this work is to study the crystallization of n-paraffins in real middle distillates, as well as the impact of alternative fuels. For that, it was proposed to expand the analytical devices used for monitoring crystallization, and to rely on models of crystallization kinetics. Crystallization studies of middle distillates were carried out using the polythermal

method using turbidimetry to detect the nucleation onset and dissolution end. Thermal-optical microscopy was used to study the crystal growth, and to link the thermal effects to the morphological changes.

2. Theory

From a thermodynamic point of view, the wax formation consists in a solid-liquid equilibrium where the n-paraffins act as solutes and all the other compounds as solvents.[9-11] Ideally, at a given temperature, the solute should include all the species which, in the pure state, have a melting point higher or equal to that temperature.[12-13] The considered solvent is a typical one that mimics the paraffin based, aromatic and oil-like solvents, and does not crystallize at the studied temperatures.

Several theories have been introduced to rationalize the nucleation and growth kinetics, however the complexity of the process and experimental limitations difficult their application to data analysis in most cases. Therefore, empirical approaches are most often preferred to analyse the crystallization kinetics, most of them initially based on the classical nucleation theory.[14]

2.1 Solubility

The saturation curve and metastable zone width are essential tools since the shape of the solubility curve defines the crystallization mode and the supersaturation conditions. The solubility curve, representing the equilibrium curve (equilibrium temperature vs concentration percentage of solute in solution), should be independent of the heating rate. However, the heating rate will influence the supersaturation and therefore the kinetics and MSZW. If the dissolution temperature is plotted against the heating rate for different mixtures which have the same solvent

but different solute concentration, the best straight lines through these points could be extrapolated to zero. This will allow to obtain the saturation temperatures at an infinitesimally small rate of temperature change, and like that the equilibrium curve (solubility).[7,8]

If the log of the solubility, in mole fraction (x), is plotted against the inverse of the absolute temperature (T), the dissolution enthalpy (ΔH_{diss}) and entropy (ΔS_{diss}) can be determined by fitting the solubility data to the van't Hoff equation, assuming ideal behaviour and negligible heat capacity difference between the solute and the solvent.[15,16]

$$\ln x = -\frac{\Delta H_{dissolution}}{RT} + \frac{\Delta S_{dissolution}}{R} \qquad (1)$$

where R is the ideal gas constant. The van't Hoff equation provides a robust thermodynamic model for single-components dissolved in organic solvents at low mass fractions. When applied to polydispersive distributions, significant uncertainty may exist in the solubility because only the highest paraffins contribute to the crystal, while the other components remain in the liquid phase at the nucleation point. For the scope of this work, this approximation can be acceptable, but a better approximation of solubilities could be obtained from the general solid-liquid equilibrium equation that relies on the composition of solute in solid and liquid phases.[9,17,18]

2.2 Classical Homogeneous Nucleation Theory

The kinetics of paraffin gel formation was studied by Paso et al.[15] using model fluids consisting of monodisperse and polydisperse n-paraffin components dissolved in petroleum mineral oil. Even if in the majority of industrial applications is the heterogeneous primary nucleation that dominates (almost inevitable presence of pollution and insoluble), these authors considered that for simple model fluids, the nucleation mechanism is homogeneous. The homogeneous nucleation of n-paraffins constitutes a special case which occurs spontaneously

and randomly throughout the bulk melt, and is not initiated by any extrinsic agents such as surfaces or impurities.[19] So, the same will be considered for real systems, complex multi-component hydrocarbon fuels, in order to apply the classical homogeneous nucleation theory.

The main equations related to the homogeneous nucleation theory can be found elsewhere.[7] The supersaturation (S) definition in mole fraction is given by:

$$\ln S = \frac{\Delta H_{diss}}{R}\left(\frac{1}{T} - \frac{1}{T_s}\right) \qquad (2)$$

where T_s is the saturation temperature. Paso et al.[15] defined the working equation for correlating the classical homogeneous nucleation theory with the experimental measured nucleating points expressed as ΔT (difference between the dissolution and nucleation temperatures, also known as metastable zone width):

$$\frac{A}{\rho^*}\Delta T\left[\exp\left(-\frac{B}{\Delta T^2}\right) - \frac{\sqrt{B\pi}}{\Delta T}erfc\left(\frac{\sqrt{B}}{\Delta T}\right)\right] = \beta \qquad (3)$$

where β is the cooling rate. The values of B and $\frac{A}{\rho^*}$ are fitting parameters obtained by least-squares minimization procedure. Knowing B and v, the value of interfacial tension γ can be estimated.

2.3 Nývlt Law

If the considered section of the metastable zone is not too large, it is reasonable to suppose that the saturation and supersaturation lines are linear and parallel, and consequently the nucleation rate equals the rate of solution supersaturation, at least when nucleation is detected. Combining these hypotheses to the principles of the homogeneous nucleation rate:

$$\log \Delta T = \frac{1-n}{n} \log \frac{dC^*}{dT} - \frac{1}{n} \log k_n + \frac{1}{n} \log \beta \qquad (4)$$

According to this equation, commonly known as Nývlt's approach,[21] the representation of $\log(\Delta T)$ against $\log\beta$ will render a straight line which slope and intercept are related to the nucleation order n and the rate constant of the crystallization k_n, respectively. n describes the dependence of the nucleation rate to the supersaturation (potential of a solute/solvent system to nucleate quickly); k_n describes the dependence of the nucleation kinetics on the solute nature (a solute which has a higher intrinsic nucleation kinetics will have a higher k_n). For organic crystallizing systems, the value of the nucleation order (n) is typically between 5 and 10.[16,20]

In spite of some severe underlying approximations, for industrial applications, this is a simple and useful way of characterizing systems and their crystallization kinetics based in a material balance made in a closed mixed vessel where the supersaturation is assured by cooling.[21]

2.4 Growth kinetics

A basic expression is used to express the relationship between supersaturation and crystal growth:

$$G = k_G \Delta C^g \qquad (5)$$

where G is the linear crystal growth rate (length/time) and, g is the crystal growth apparent order (temperature-dependent) and is normally a number between 1 and 2.[7] There are a number of experimental methods that can be used to obtain the crystal growth rate data needed to obtain kinetics, such as induction time measurements[22] or droplet based microfluidic[23].

3. Materials and Methods

3.1 Materials

In this work, three types of fuels with different distillation ranges and paraffin levels (heavy, light, and distillate hydrocracker (DHC)) are used to prepare different diesels (B0). Table 1 shows the characteristics of each one, as well as those of the heating fuels studied (FOD1 and FOD2) for comparison. To prepare different blends of 7%vol ester in the middle distillates (B7), esters from different sources are mixed, and their nature and quantity are reported in Table 2.

Two standard mixtures were prepared from the original fuels, B0 and B7, and from them, several other mixtures were prepared with different percentages of fuels, keeping the solvent constant (aromatics, naphthenes,…) but changing the n-paraffins mass percentage and their paraffinic profile. The mixtures are denominated from B0 to B0 8, and from B7 to B7 6 for the mixtures containing esters (FAME). The compositions of these mixtures were calculated by a weighted average, considering the composition of each original fuel and the formulation of each mixture. The n-paraffin content of each mixture is presented in Table 3.

3.2 Nucleation experimental set-up

The crystallization reactor consists in a triple-wall jacketed 50cm^3 glass vessel which has ports to accommodate the turbidity and temperature probes. A magnetic stirrer (IKA-WERK ES5) is used to agitate the solution where a speed of 400 rpm is applied which ensures an adequate mixing and avoids excessive splashing in the vessel. Cooling and heating programmes are implemented using a cryothermostat (LAUDA Kryomat RUK 90S). Temperature data are recorded using a Pt100 resistance probe which is immersed in the solution and is connected to the cryothermostat.

The turbidity probe introduces light into the reactor from a light source (Avantes AvaLight DHS) and collects the dispersed light which is then analysed (Avantes Multichannel Spectrophotometer). A fiber optics system connects the probe to the light source and spectrophotometer. In this work, the scattered light intensity was analysed in the wavelength range between 450 and 655 nm.

The crystallization reactor is initially loaded with approximately 20 cm^3 of the sample, and stirring is started at the desired rate (400 rpm). The solution is first heated until 35°C to ensure complete dissolution and minimize memory effects. The solution is then cooled, at a fixed cooling rate, until a temperature just below the appearance of the first crystals. The formation of crystals is accompanied by a rapid increase of the scattered light intensity. Then, a heating ramp is imposed, at the same rate used in the cooling, until complete dissolution (35°C). The value at which the scattered light intensity increases is taken as the nucleation temperature, while that at which it decreases, is taken as the "equilibrium" saturation temperature (dissolution). The procedure is repeated for different cooling/heating rates (2, 10, 30 and 60°C/hr), and at least three measurements are done at each rate. To minimize the amount of sample consumed, the same solution is recycled batch to batch.

3.3 Thermomicroscopy

A microscope (LEICA DM RXA) equipped with a polarized light and a phase contrast device was used. It is connected to a hot stage (Linkam Optical DSC600), which can operate in the range from -150 to 600°C controlled by a cooling system (LNP95). The heat/cooling rates are limited to 6 to 1800°C/hr, with a precision of 0.01°C. Images are acquired using a sensitive charge-coupled device colour camera (PCO Sensicam QE).

The solution is placed in a quartz crucible (15mm diameter and 20µl), and a cooling rate is imposed, without any stirring. Image acquisition is done simultaneously. The linear growth rate can be obtained by measuring the largest crystal dimension (the width) as a function of time (and temperature). A standard cooling rate of 0.5°C/min is used and at least ten crystals are followed to study the crystal growth rate.

4. Results and Discussion

When cooling a diesel (B0), the solute is considered to be the n-paraffins while the other components constitute the solvent. In the case of mixtures diesel/FAME (B7), the saturated esters are considered as solute as well. The solvent includes: isoparaffins, naphthenes, iso-naphtehnes, di-naphthenes, mono-, di-, tri- and poly-aromatics, monoaro- and diaro-naphthenes, and a mass percentage lower than 0.1% of other components, as showed in Table 1 for the different fuels.

As mentioned before, several different mixtures were prepared from different fuels. A mixture law was used to calculate their composition: knowing the density, volume percentage and composition of pure fuels, and the formulation of the mixture, its composition can be calculated. Experimental data of the composition of each mixture was compared to the estimated values, and the standard deviations are negligible: considering the n-paraffins, the standard deviation is in average 2.42% which can be considered a very good agreement.

The molecular weight (M) of each mixture was calculated by a weighted average considering the estimated mixture composition and the molecular weight of each component. From the density of each fuel and the formulation of each mixture, the mixture density (ρ) was estimated. Knowing M and ρ, the molar volume (v) was estimated. These values together with the

concentration of n-paraffins are presented in Table 3, and they are in good agreement with available literature values.[24] The values of M, ρ and v are quite similar for all the studied mixtures, even if the quantity of n-paraffins and their profile are changed.

4.1 Blends diesel/biodiesel and heating fuels

The nucleation, T_n, and dissolution, T_s, temperatures were measured for the different mixtures, and the respective differences (ΔT) are presented in Figure 1 and Figure 2, respectively for diesels and biodiesels. These values are averages of at least three different measurements, and the standard deviation in the absolute temperatures ranges between 0 and 11%. As expected, the dissolution temperature is always higher than that of nucleation, and the difference between them is higher at the highest rates. However, in both nucleation and dissolution, the rate has not a great effect, and they can be considered almost constant as a function of cooling/heating rate. Initially, seven different rates were tested, but as it was found that the rate has not a remarked effect, only four rates were studied for the other samples. Turnbull and Cormia[25] showed that from C_{16} to C_{32} the relative undercooling for homogeneous nucleation, $\Delta T/T_s$, is ~0.04 instead of the ~0.2 common to most organic materials. The samples studied in this work have $\Delta T/T_s$ between 0.008 and 0.013, which means that in the case of real systems the maximum undercooling is lower than for model systems.

These diesels are mixtures of three different fuels, and highest the ratio light to heavy, lower the nucleation and dissolution temperatures, as in the cases of B0 5, B0 8, B7 3 and B7 5 where the quantity of light fuel is especially high. The quantity of DHC also plays an important role: higher it is, higher the temperatures, as in the case of B0 7 where the same quantity of heavy and DHC is used.

The values obtained for the standard B0 are in good agreement with the commonly found for traditional diesels.[3,26] In addition, the type of curves found are similar to those found for model systems like octacosane/toluene, but with very different dissolution and nucleation temperatures. Comparing the nucleation temperatures of the mixtures B7, with values available in the literature for traditional biodiesels,[4,27] it can be seen that the blends diesel/esters prepared in this work have better cold flow properties (lower cloud points).

Comparing the mixtures based on B0 and the corresponding B7 (it means that the quantity of light and DHC fuels are the same), it can be seen that the temperatures are in the same range, as well as the order by which the samples are classified: for example, B0 5 and B7 3 are the ones with lower nucleation and dissolution temperatures; while B0 2 and B7 2 have the higher. This means that the quantity of esters has almost no influence on the nucleation, being the n-paraffin quantity the major parameter playing a role. This was kind expected since in Table 3 it can be seen that the esters had a maximum total saturated FAME content of 12% which means that blending the middle distillates with 7%vol esters meant that the total saturated FAME content was less than 1%, in any of the blends.

The heating fuels (FOD1 and FOD2) have considerable worst cold flow properties: from 1.4 and -0.4°C for the nucleation temperature; and from 3.40 to 2.55 for the dissolution. The final distillation temperature of a FOD is higher than that of a conventional diesel: this means that there are more dissolution of the lighter paraffins and so the heavier will be more concentrated in FOD, causing problems in cold temperature behaviour. The paraffins distribution in FOD is bimodal and centred between C_{11} and C_{17}, while for the conventional diesels is centred in C_{16}. The amount of n-paraffins is higher in a conventional diesel but especially rich in light paraffins which crystallize at lower temperatures what will make the nucleation temperature to be lower.

4.3 Effect of concentration

The solubility curves, expressed in concentration of solute, are shown in Figure 3, for the mixtures based in B0 and for those based in B7. This is the first time that the solubility curve is measured for that kind of complex systems. It should be focused that the difference on the solubility curve slopes between B0 and B7 is negligible and so the esters have a slightly effect on the solubility slopes.

The concentrations in g/100g were converted in mole fraction considering the molecular weight of solute and solvent. This allowed the application of the empirical van't Hoff approach even if this corresponds to a great simplification. The results of the dissolution properties are presented in Table 4: the difference between B0 and B7 values are negligible, as expected since the same was seen in the solubility slopes.

If the obtained values are compared with literature values for model systems, like monodisperse and polydisperse *n*-paraffins dissolved in mineral oil[4,15] for real systems the values are lower: the quantity of components in the solute and the solvent makes the interactions to be weaker and so, the quantity of energy needed to broke them is lower. The dissolution enthalpy is associated with the dissolution of a substance in a solvent at constant pressure resulting in infinite dilution. The energy change can be regarded as the endothermic breaking of bonds within the solute and within the solvent, followed by the formation of attractions between the solute and the solvent. So, these values are very dependent on the solute and solvent interactions.

4.4 Nucleation kinetics

Applying the equations presented in section 2.2, to relate the critical undercooling measured through a polythermal approach as a function of cooling rate, an estimation of the crystal-solution interfacial tension was done which is considered as crystal face and temperature independent. The values of B and A/ρ^* are obtained for each cooling rate, and the standard deviation between them was lower than 5%. So, another minimization was done of all the least-squares corresponding to a mixture, and fixed B and A/ρ^* for a given mixture were obtained. This led to a single interfacial tension, cooling rate independent, presented in Table 3. The supersaturation presented is that estimated at 1°C/min because this is the common rate used for the measurements of the filtering limit temperature. The presence of FAMEs makes the supersaturation at nucleation and the interfacial tension to increase, as well as the critical radius and consequently the Gibbs energy. The composition of the mixtures changed, including the saturated, aromatic, resin and asphalthenes fractions. And so, the interactions between the polar functional groups are changed which are important to its structure and characteristics.

It is known that the constraints on the liquid chains connected to the critical nucleus yield an entropic cost and, therefore, an increase of the interfacial tension.[28] Kraack et al.[19] estimated the solid-liquid interfacial tensions of *n*-paraffins from 17 to 60 dyn/cm, and the values found in this work are considerably lower than theirs. Gerson et al.[8] determined the interfacial tension from the induction time of docosane crystallized from dodecane and the values are lower than the found in this work, even if in the same order. The same happens in comparison to the values determined by Paso et al.[15] for monodisperse C_{36} and C_{35} and polydisperse n-paraffin components dissolved in petroleum mineral oil.

Three main variables govern the nucleation rate: temperature; supersaturation; and interfacial tension. The values of supersaturation and interfacial tension were presented in Table 3. In the

impossibility of performing molecular simulations to establish the nuclei structure, a constant A value equal to 10^{30} nuclei/cm^3.s was considered.[20] Consequently, the nucleation rate was calculated and represented as a function of supersaturation. As shown in Figure 4a, there is an extremely rapid increase in the nucleation rate for B0 once some critical supersaturation level is exceeded, being the one with higher nucleation rates. It can be seen that to obtain the same nucleation rate, higher supersaturation is required in the cases if B7 and FOD when compared to B0, which means lower temperatures and better flowability. This means that for B7 and FOD be used in the same conditions as B0, some additives should be added.

This can be ensured if a comparison is made between the mixtures prepared from B0 and the corresponding from B7. The first have higher nucleation rates, and so higher number of nucleus per unit of volume and time, than the corresponding mixtures prepared from B7 (Figure 4b). Those mixtures have exactly the same quantity of heavy and DHC fuels, being the quantity of light fuel slightly lower in the B7 mixtures given that they are blended with 7%vol of esters. It clearly appears from these figures that the presence of alternative fuels lengthens the nucleation rate.

The previous analytical approach based on the classical nucleation theory allowed to obtain a characteristic parameter of the interactions crystal-solution. Even if the nucleation rate was also obtained using this approach, another empirical approach was used to describe nucleation kinetics, the Nývlt law (section 2.3). The application of equation (4) leads to two empirical parameters, n and k_n, and the first aim of its application is to determine those values, considering the solubility curve slopes presented in Figure 3. The uncertainties in the solubility curves slopes are so low that they have no effect on the kinetic parameters presented in Table 3. For the mixtures studied in this work, the behaviour is similar to conventional organic systems, given

that n is between 5 and 10, including those of the studied FODs. In general, the kinetic parameters in the presence of FAMEs are higher. In general, the lower the solubility of a solute in a given solvent, the higher is the value of n, and higher the nucleation temperature. This means that it is a useful parameter to assess the effect of different solvents or solvent compositions on the metastability of a solution: given that in the presence of FAME it is higher, this means that those mixtures have higher nucleation temperatures, and consequently the applicability of those fuels is not possible unless some cold behaviour treatment is applied.

It should be mentioned that for the FODs the same solubility curve as B0 was considered, as well as the molecular volume and dissolution enthalpy. This can cause deviations from the real behavior, and the obtained results with models for FOD are just for comparison.

4.5 Experimental Growth Rate

Claudy and Letoffé[29,30] used optical microscopy in polarized light to study the crystallization of n-paraffins in middle distillates and they concluded that it is the most appropriate mode to observe paraffin crystallization. The crystals obtained in this work are plate-like with a high aspect ratio and a lozenge shape. Images of three different samples are presented in Figure 5.

The linear crystal growth rate was measured for each different mixture based on at least ten different crystals, and the results are presented in Table 3, together with the crystal size (width, L) a time delay after nucleation (30-50s). Experimentally it was seen that the presence of FAMEs has not a remarked effect on the crystal size but generally increases the crystal growth rate. The nature of the solvent plays an important role in the growth, since the FODs have considerably higher growth rates.

At low supersaturation, crystals can grow faster than they nucleate resulting in a bigger crystal size and narrow crystal size distribution. However, at higher supersaturation, crystal nucleation dominates crystal growth, ultimately resulting in smaller crystals and broad crystal size distribution. As seen before, the FODs have lower supersaturation at nucleation than the other mixtures, and here it was found that they have higher growth rates as well as bigger crystals. In opposition, B0 have a slightly higher supersaturation at nucleation, and a lower growth rate as well as smaller crystals.

Considering a metastable zone sufficiently thin that the saturation and supersaturation curves are linear and parallel and the growth predominates over nucleation, the supersaturation is converted in temperature difference. So, if the linear growth rate was measured at different cooling rates, and consequently the ΔT estimated, the values of k_G and g can be obtained by linearization of equation (5). The results for B0 and B7 are presented in Table 5 where it could be seen that the growth rate increases when the cooling rate increases. However, the maximal size of the crystals is almost not affected. The growth order g increases with the growth rate and also with the metastable zone width. As mentioned before, for common organic systems the value of g should be between 1 and 2 what means that B0 and B7 can be considered as common organic systems.

5. Conclusions

The aim of this work was to study crystallization kinetics for middle distillates, in order to better understand their cold flow behaviour. Firstly, a mixture law was used to calculate the paraffin contents of a mixture based on those of its constituting fuels. The concentration of interest will be those of n-paraffins (10<C<50 g/100g) and, concerning these species the standard

deviation between measured and estimated concentrations is 3.2% which corresponds to a very good agreement. The solute was defined as the n-paraffins and the saturated esters; all the other components (naphthenes, asphalthenes, aromatics) were considered as solvent. Different mixtures were prepared from two standard mixtures, keeping the solvent and changing the paraffins mass percentage and their paraffinic profile.

An experimental device was set-up to measure dissolution and nucleation temperatures and it was verified that the cooling/heating rate has a negligible effect on the nucleation/dissolution temperatures. Solubility curves were obtained for the first time for such complex systems. It was seen that the esters have no influence on the solubility, but if the nature and source of esters are different the effects can be different. The incertitude of the solubility curve slopes is so small that there is no effect on the kinetic parameters.

The application of the homogeneous nucleation theory allow to calculate the nucleation rate as a function of the supersaturation what show that concerning the nature of the sample the nucleation will be different. The interfacial tension between crystal and solution for the different studied samples was obtained what allows distinguishing between samples. The Nývlt law was applied to obtain the kinetic parameters, and it was seen that the order of nucleation is similar for all the studied samples and they could be considered as normal organic systems. The applicability of some studied mixtures as fuels will be possible just in case of cold flow treatment for example with some additives.

A second experimental device was introduced to study the crystal growth rate. All the studied samples have crystals of the same shape (plate-like) only changing the size and the supersaturation at nucleation. The linear crystal growth rate changes concerning the nature of the

sample. A kinetic growth rate law was obtained for samples with and without esters, being the apparent order of growth higher in the absence of esters.

Nomenclature

A	pre-exponential factor or collision factor
B	fitting parameter
g	crystal growth apparent order
G	overall linear growth rate
J	nucleation rate
k_n	nucleation rate constant
k_G	growth rate constant
L	characteristic size of the crystal
M	molecular weight
n	apparent order of nucleation
r	radius
R	ideal gas constant
S	supersaturation
T	temperature
v	molar volume
x	solubility, in mole fraction

Greek letters

β	cooling rate
γ	interfacial tension
ρ	density of the mixture can be estimated
ρ^*	critical nuclei number density (fitting parameter)
ΔC	MSZW for a given temperature (in mass of solute per mass of solvent)
ΔH	enthalpy
ΔS	entropy

ΔT	maximum undercooling
$\Delta T/T_s$	normalized metastable zone
Subscripts	
c	*critical*
diss	dissolution
s	dissolution
n	nucleation
Abbreviations	
B0	diesel
B7	mixture diesel/biodiesel
CP	cloud point
DHC	fuel coming from new refinery schemas
FAME	fatty acid methyl esters
FOD	heating fuels
MSZW	metastable zone width

References

(1) Papin, G. Synthèse, caractérisation et évaluation de nouveaux additifs de tenue à froid des gazoles et fiouls domestiques, Bordeaux; 2008.

(2) Dunn, R.O. Crystallization behavior of fatty acid methyl esters. *Journal of the American Oil Chemists Society* **2008**, *85*, 961-972.

(3) Knothe, G.; Dunn, R.O. A Comprehensive Evaluation of the Melting Points of Fatty Acids and Esters Determined by Differential Scanning Calorimetry. *Journal of the American Oil Chemists Society* **2009**, *86*, 843-856.

(4) Lopes, J.C.A.; Boros, L.; Krahenbuhl, M.A.; Meirelles, A.J.A.; Daridon, J.L.; Pauly, J.; Marrucho, I.M.; Coutinho, J.A.P. Prediction of cloud points of biodiesel. *Energy & Fuels* **2008**, *22*, 747-752.

(5) Sarin, A.; Arora, R.; Singh, N.P..; Sarin, R.; Malhotra, R.K.; Kundu, K. Effect of blends of Palm-Jatropha-Pongamia biodiesels on cloud point and pour point. *Energy* **2009**,*34*, 2016-2021.

(6) Senra, M.; Paracharoensawad, E.; Scholand, T.; Fogler, H.S. Role of a Carboxylic Acid on the Crystallization, Deposition, and Gelation of Long-Chained n-Alkanes in Solution. *Energy & Fuels* **2009**, *23*, 6040-6047.

(7) Mullin, J.W. Crystallization, Fourth ed., Oxford,Butterworth-Heinemann, 2001.

(8) Gerson, A.R.; Roberts, K.J.; Sherwood, J.N.; Taggart, A.M.; Jackson, G. The Role of Growth Environment on the Crystallization of Normal Alkanes in the Homologous Series from C18h38 to C29h60. *Journal of Crystal Growth* **1993**, *128*, 1176-1181.

(9) Coutinho, J.A.P.; Goncalves, C.; Marrucho, I.M.; Pauly, J.; Daridon, J.L. Paraffin crystallization in synthetic mixtures: Predictive local composition models revisited. *Fluid Phase Equilibria* **2005**, *233*, 28-33.

(10) Coutinho, J.A.P.; Mirante, F.; Ribeiro, J.C.; Sansot, J.M.; Daridon, J.L. Cloud and pour points in fuel blends. *Fuel* **2002**, *81*, 963-967.

(11) Daridon, J.L.; Pauly, J.; Coutinho, J.A.P.; Montel, F. Solid-liquid-vapor phase boundary of a North Sea waxy crude: Measurement and modeling. *Energy & Fuels* **2001**,15, 730-735.

(12) Coutinho, J.A.P. Predictive UNIQUAC: A new model for the description of multiphase solid-liquid equilibria in complex hydrocarbon mixtures. *Industrial & Engineering Chemistry Research* **1998**, *37*, 4870-4875.

(13) Dauphin, C.; Daridon, J.L.; Coutinho, J.A.P.; Baylere, P.; Potin-Gautier, M. Wax content measurements in partially frozen paraffinic systems. *Fluid Phase Equilibria* **1999**, *161*, 135-151.

(14) Nývlt, J. Kinetics of nucleation in solutions. *Journal of Crystal Growth* **1968**, *3-4*, 377-383.

(15) Paso, K.; Senra, M.; Yi, Y.; Sastry, A.M.; Fogler, H.S. Paraffin polydispersity facilitates mechanical gelation. *Industrial & Engineering Chemistry Research* **2005**, *44*, 7242-7254.

(16) Ashbaugh, H.S.; Radulescu, A.; Prud'homme, R.K.; Schwahn, D.; Richter, D.; Fetters, L.J. Interaction of paraffin wax gels with random crystalline/amorphous hydrocarbon copolymers. *Macromolecules* **2002**, *35*, 7044-7053.

(17) Coutinho, J.A.P.; Daridon, J.L. Low-pressure modeling of wax formation in crude oils. *Energy & Fuels* **2001**, *15*, 1454-1460.

(18) Coutinho, J.A.P.; Knudsen, K.; Andersen, S.I.; Stenby E.H. A local composition model for paraffinic solid solutions. *Chemical Engineering Science* **1996**, *51*, 3273-3282.

(19) Kraack, H.; Sirota, E.B.; Deutsch, M. Measurements of homogeneous nucleation in normal-alkanes. *Journal of Chemical Physics* **2000**, *112*, 6873-6885.

(20) Myerson, A.S. Handbook of Industrial Crystallization 2ed., Woburn, MA, 2002.

(21) Nývlt, J. The Kinetics of industrial crystallization, New York, 1985.

(22) Teychené, S.; Biscans, B. Nucleation Kinetics of Polymorphs: Induction Period and Interfacial Energy Measurements. *Crystal Growth & Design* **2008**, *8*:1133-1139.

(23) Teychené, S.; Biscans, B. Crystal nucleationinadropletbasedmicrofluidiccrystallizer. *Chemical Engineering Science* **2012**, *77*:242-248.

(24) Mesquita, F.M.R.; Feitosa, F.X.; Santiago, R.S.; de Sant'Ana, H.B. Density, Excess Volumes, and Partial Volumes of Binary Mixtures of Soybean Biodiesel plus Diesel and

Soybean Biodiesel plus n-Hexadecane at Different Temperatures and Atmospheric Pressure. *Journal of Chemical and Engineering Data* **2011**, *56*:153-157.

(25) Turnbull, D.; Cormia, R.L. Kinetics of Crystal Nucleation in Some Normal Alkane Liquids. *The Journal of Chemical Physics* **1961**, *34*:820-831.

(26) Gimzewski, E.; Audley, G. Monitoring Wax Crystallization in Diesel Using Differential Scanning Calorimetry (Dsc) and Microcalorimetry. *Thermochimica Acta* **1993**, *214*:149-155.

(27) Coutinho, J.A.P.; Goncalves, M.; Pratas, M.J.; Batista, M.L.S.; Fernandes, V.F.S.; Pauly, J.; Daridon, J.L. Measurement and Modeling of Biodiesel Cold-Flow Properties. *Energy & Fuels* **2010**, *24*:2667-2674.

(28) Kraack, H.; Deutsch, M.; Sirota, E.B. n-alkane homogeneous nucleation: Crossover to polymer behaviour. *Macromolecules* **2000**, *33*:6174-6184.

(29) Claudy, P.; Letoffe, J.M.; Bonardi, B.; Vassilakis, D.; Damin, B. Interactions between N-Alkanes and Cloud Point Cold Filter Plugging Point Depressants in a Diesel Fuel - a Thermodynamic Study. *Fuel* **1993**, *72*:821-827.

(30) Létoffé, J.M.; Claudy, P.; Kok, M.V.; Garcin, M.; Volle, J.L. Crude Oils - Characterization of Waxes Precipitated on Cooling by Dsc and Thermomicroscopy. *Fuel* **1995**, *74*:810-817.

Table 1. Original fuel characteristics.

	Heavy	Light	DHC[1]	FOD 1[2]	FOD 2
Viscosity (mm^2/s)	2.629	1.216	4.916		
Density (kg/m^3)	831.7	807.6	837.0	860.9	858.0
Flash point (°C)	61	45	113	64	63
Cloud point (°C)	-7.0	-34.0	5.0	0	-1
Paraffin			**%m/m**		
n-Paraffins	21.54	16.73	15.39	11.15	13.06
Isoparaffins	24.14	27.71	31.56		
Naphthenes	3.76	3.66	4.31		
Isonaphthenes	15.13	19.07	20.34		
Dinaphthenes	6.45	8.61	6.22		
Monoaromatics	12.00	14.37	9.71		
Diaromatics	4.26	1.54	2.60		
Triaromatics	0.61	0.06	0.47		
Polyaromatics	0.09	0.00	0.49		
Monoaronaphthenes	9.97	7.99	7.68		
Diaronaphthenes	2.05	0.27	1.08		
Others	0.00	0.00	0.13		

[1]DHC, fuel coming from new refinery schemas; [2]FOD, heating fuel

Table 2. FAME analysis of the oil used to prepare B7.

Fatty acid ester		m/m %
Palmitic acid	**16:0**	9.4
Palmitoleic acid	**16:1**	0.3
	17:1	0.1
Stearic acid	**18:0**	2.1
Oleic acid	**18:1**	56.4
Linoleic acid	**18:2**	20.3
Linolenic acid	**18:3**	8.6
Arachidic acid	**20:0**	0.5
Gondoic acid	**20:1**	1.1
Behenic acid	**22:0**	0.3
Erucic acid	**22:1**	0.2
Lignoceric acid	**24:0**	0.1
Nervonic acid	**24:1**	0.1
Non identified		0.6

Table 3. Solution properties, fundamental nucleation parameters, crystal size and linear growth rate of the different mixtures.

	$C_{n\text{-}paraffins}$ (g/100g)	M (g/mol)	ρ (kg/m^3)	v (dm^3/mol)	T_s (°C)	$S_{1°C/min}$	γ (dyn/cm)	r_c (A°)	n	log(kn)	L (µm)	G (µm/s)
B0	18.88	201.89	825.53	0.245	-3.74	1.22	0.89	9.97	7.50	11.3	100	0.69
B0 2	19.35	206.72	827.94	0.250	-4.17	1.21	0.77	9.05	10.0	16.4	86	0.68
B0 4	18.41	197.09	823.16	0.239	-2.63	1.12	0.39	7.14	7.25	11.7	371	6.37
B0 5	17.02	177.55	814.42	0.218	-9.29	1.19	0.99	11.68	10.9	17.7	451	5.38
B0 7	17.93	209.84	826.06	0.254	-1.49	1.17	1.28	18.99	8.16	13.1		
B0 8	17.43	187.11	818.30	0.229	-7.17	1.22	0.95	9.88	7.69	11.8	258	2.62
B7	18.68	201.74	829.07	0.243	-2.69	1.26	0.93	8.68	12.6	19.1	85	2.34
B7 2	19.19	206.32	831.48	0.248	-2.74	1.20	0.81	10.26	12.7	20.5	172	3.83
B7 3	16.67	180.41	817.96	0.221	-9.49	1.31	1.16	8.59	7.67	11.9	50	1.47
B7 4	18.39	199.45	827.96	0.241	-3.50	1.14	0.40	6.54	8.42	13.4	235	12.34
B7 5	17.12	187.72	821.84	0.228	-7.08	1.21	1.01	11.03	9.50	15.1	108	4.98
B7 6	18.16	197.11	826.66	0.238	-4.87	1.18	0.96	12.28	8.05	13.1	169	5.00
FOD1	10.55	201.89	825.53	0.245	3.06	1.15	0.88	13.9	10.2	16.6	325	4.17
FOD2	11.27	201.89	825.53	0.245	2.54	1.20	1.04	12.3	6.20	9.40	132	2.09

$C_{n\text{-}paraffins}$, concentration of normal paraffins; M, molecular weight; ρ, density; v; molecular volume; T_s, saturation temperature; $S_{1°C/min}$, supersaturation calculated at 1°C/min; γ, interfacial tension; r_c, critical radius; n, apparent order of nucleation; log(k_n), base-10 logarithm of the nucleation rate constant; L, characteristic size of the crystal; G, crystal growth rate.

Table 4. Paraffin dissolution enthalpy (kJ/mol) and entropy (kJ/mol.K) values derived from the van't Hoff Solubility relation, based on experimental dissolution points.

	B0	**B7**
$\Delta H_{dissolution}$ **(kJ/mol)**	37.84 ± 6.18	40.56 ± 3.20
$\Delta S_{dissolution}$ **(kJ/mol.K)**	0.12 ± 0.02	0.14 ± 0.01

Table 5. Linear growth rate (G) as a function of cooling rate (β), and the respective kinetic parameters, k_g and g.

		β (°C/min)					
	$S_{1°C/min}$	**0.10**	**0.17**	**0.50**	**1.00**	$\ln(k_G)$	**g**
		G (µm/s)					
B0	**1.22**	0.44	0.48	0.69	1.24	9.25	2.54
B7	**1.26**	2.05	2.20	2.54	3.22	7.80	1.90

Figure 1.Difference between dissolution and nucleation temperatures for different cooling rates, for the following diesels (experimental error <10%): ♦, B0; ■, B0 2; Δ, B0 4; x, B0 5; □, B0 7; -, B0 8.

Figure 2. Difference between dissolution and nucleation temperatures for different cooling rates for the following biodiesels (experimental error <10%): ■, B7; Δ, B7 2; x, B7 3; ○, B7 4; □, B7 5; ▲, B7 6.

Figure 3. Solubility curve of a diesel expressed in concentration of normal paraffins higher than 11 as a function of dissolution temperature: (■) B0 and (□) B7.

Figure 4. Effect of supersaturation on the nucleation rate: (a) —, B0, ---, B7, —.—, FOD, (b) mixtures prepared from B0 (—, B0; ■, B0 2; ♦, B0 5; x, B0 8; •, B0 4) and the corresponding prepared from B7 (—, B7; □, B7 2; ◊, B7 3; *, B7 5; ○, B7 6).

Figure 5. Images of crystals of different mixtures: a) B0, b) B7, and c) FOD.

Figure 1

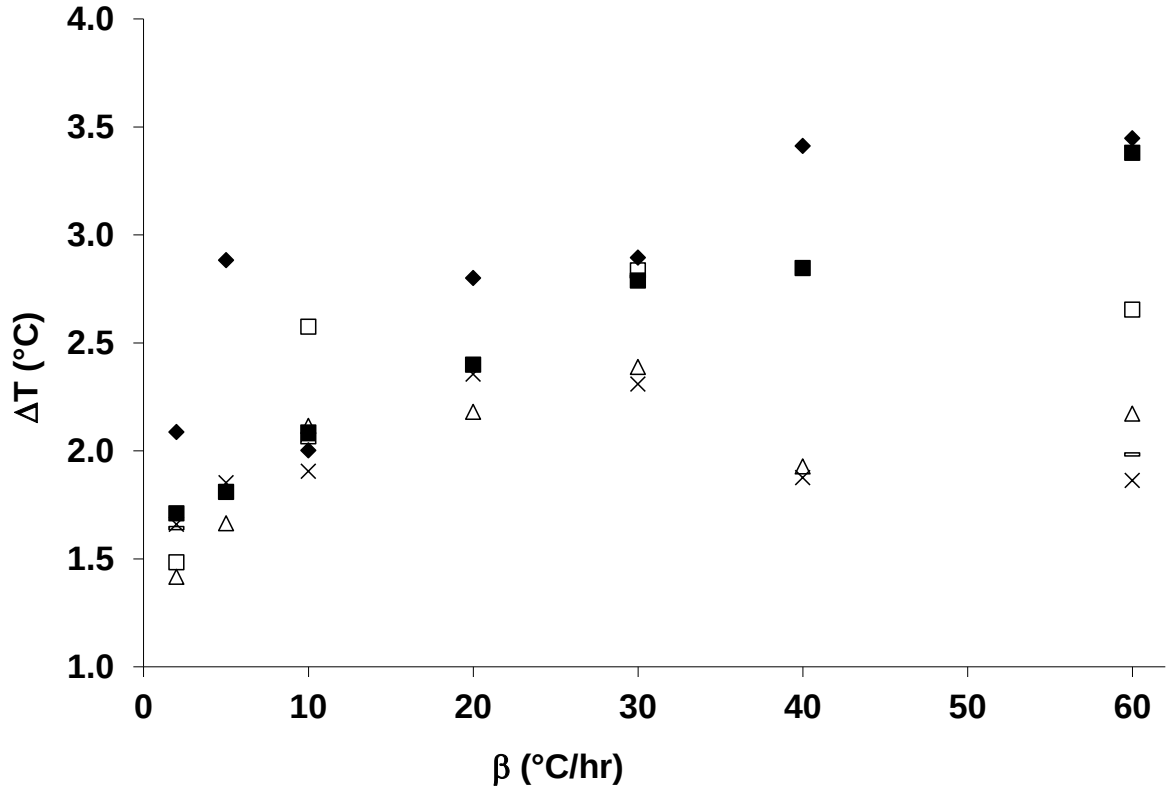

Figure 2

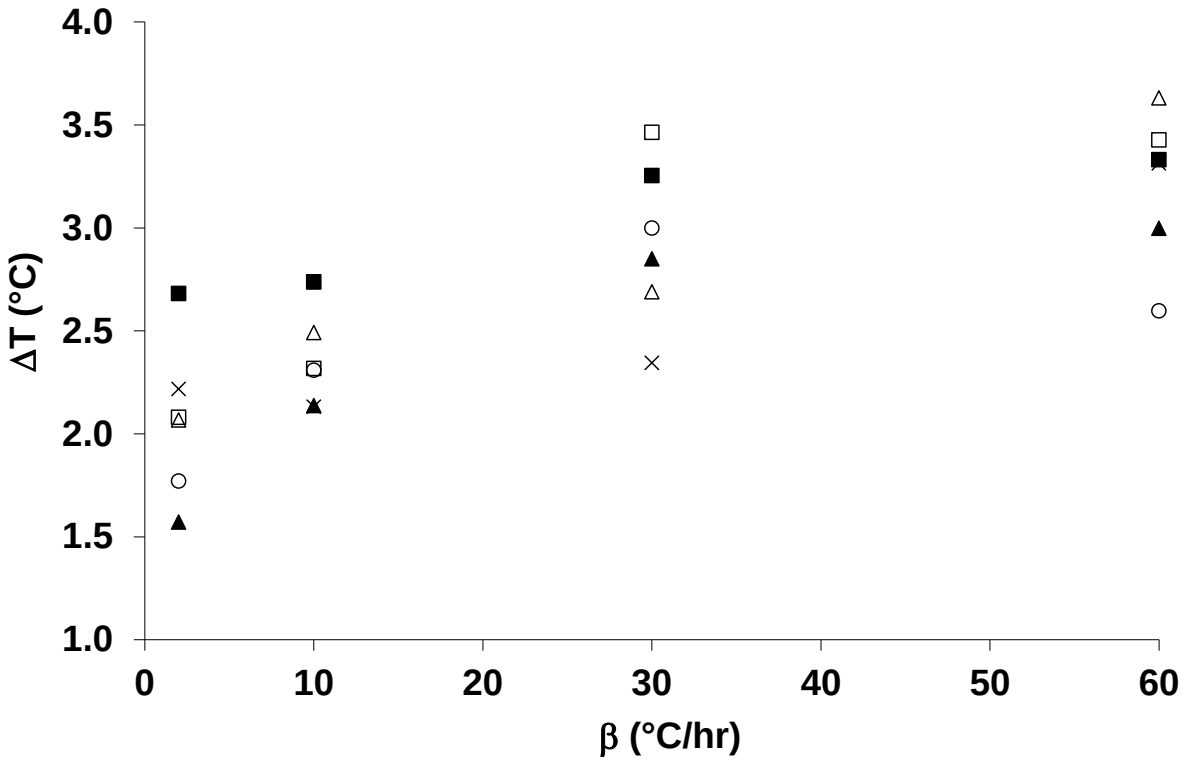

Figure 3

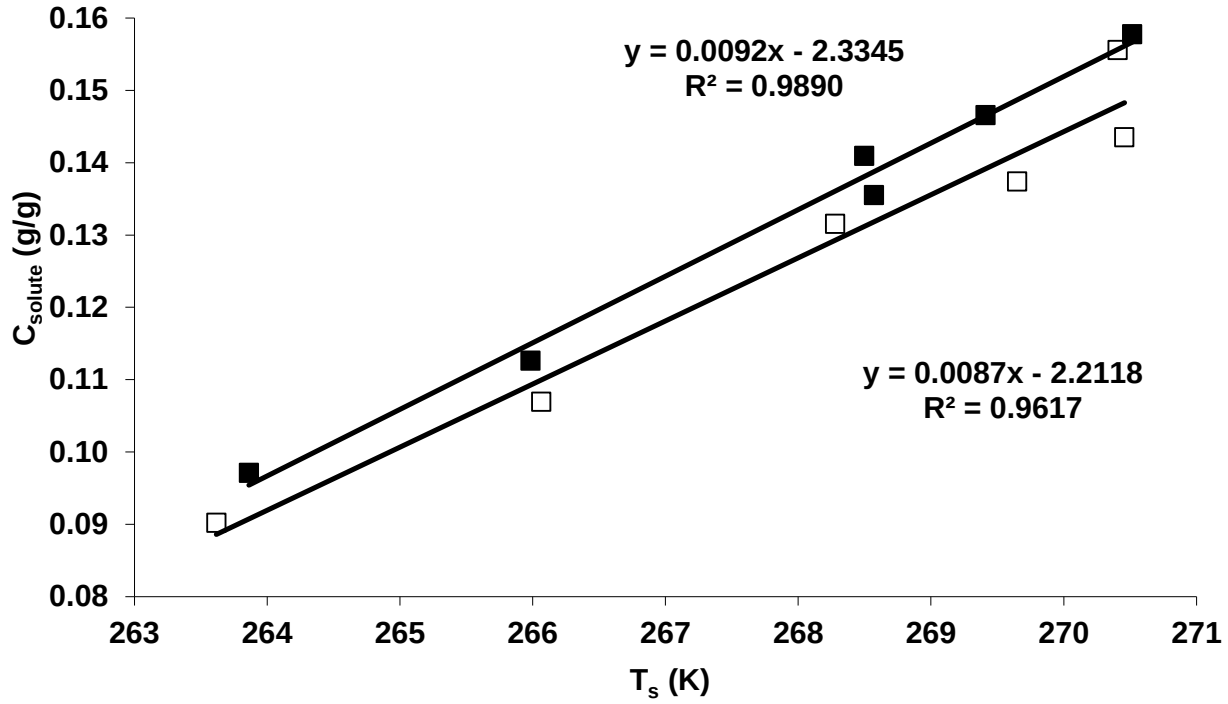
y = 0.0092x - 2.3345
R² = 0.9890
y = 0.0087x - 2.2118
R² = 0.9617
C_solute (g/g)
T_s (K)
0.16
0.15
0.14
0.13
0.12
0.11
0.10
0.09
0.08
263
264
265
266
267
268
269
270
271

Figure 4

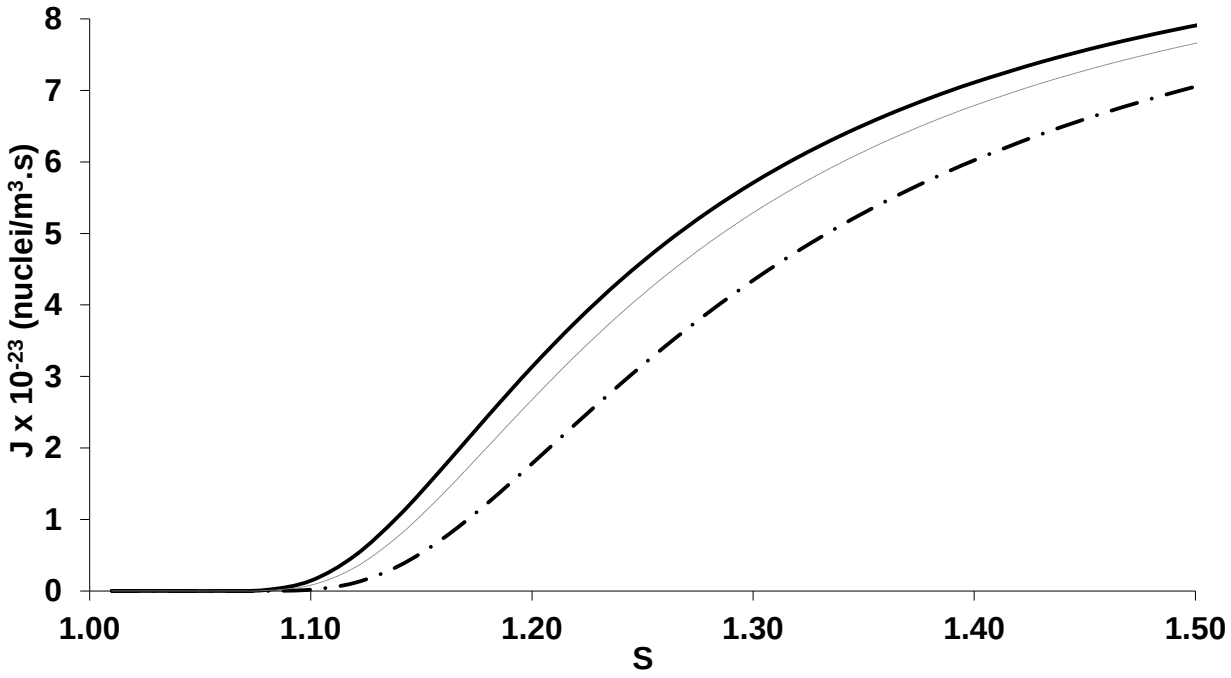
J x 10-23 (nuclei/m3.s)
S
0
1
2
3
4
5
6
7
8
1.00
1.10
1.20
1.30
1.40
1.50

(a)

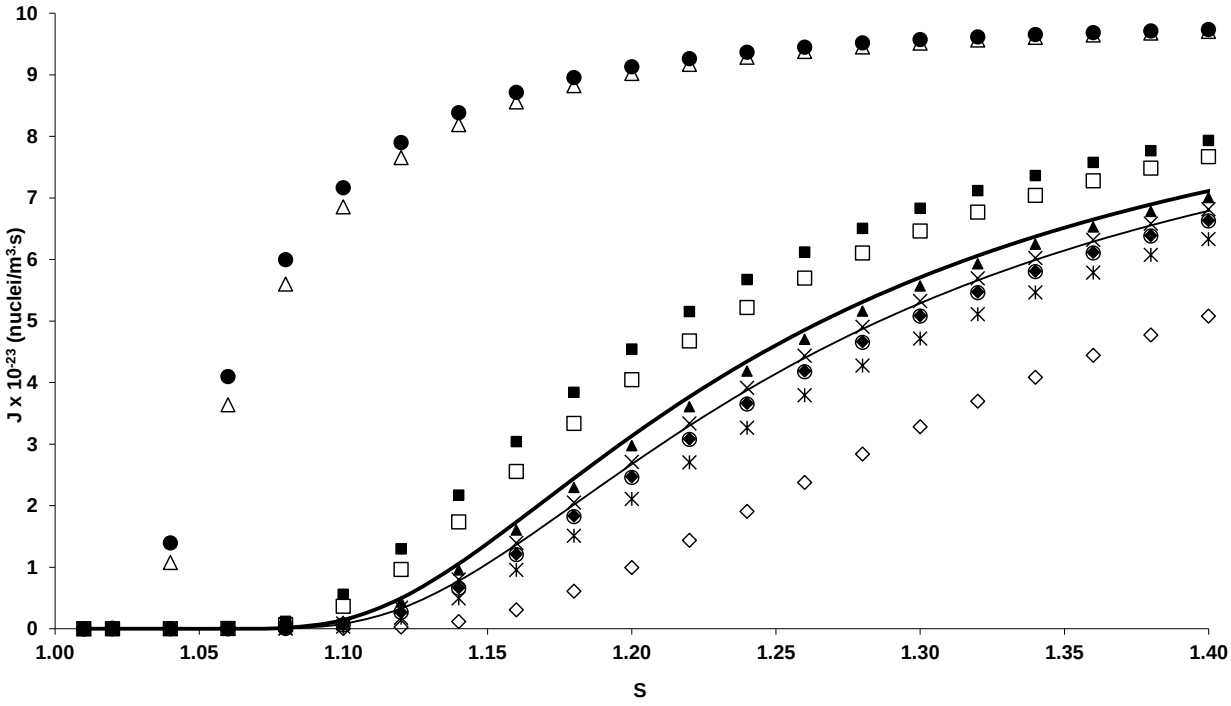
J x 10-23 (nuclei/m3.s)
S
0
1
2
3
4
5
6
7
8
9
10
1.00
1.05
1.10
1.15
1.20
1.25
1.30
1.35
1.40

(b)

Figure 5

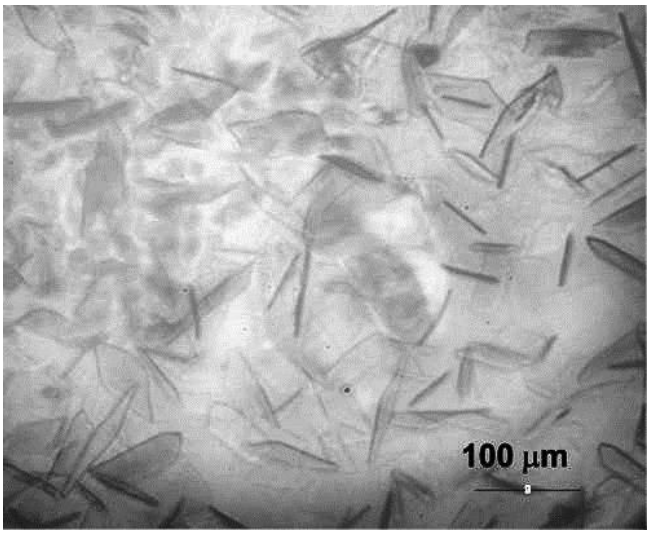

(a)

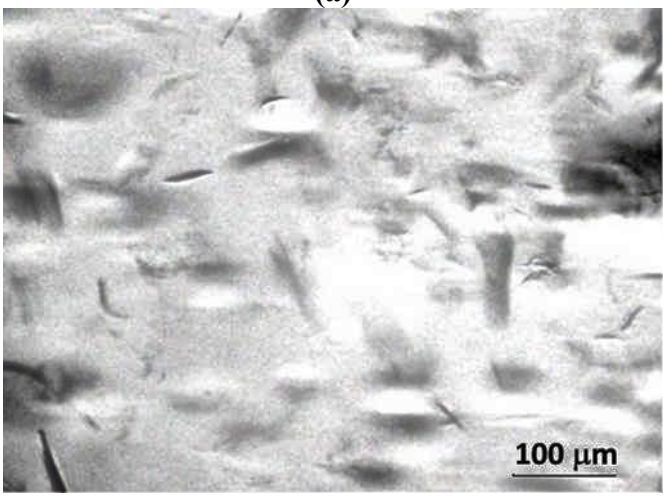

(b)

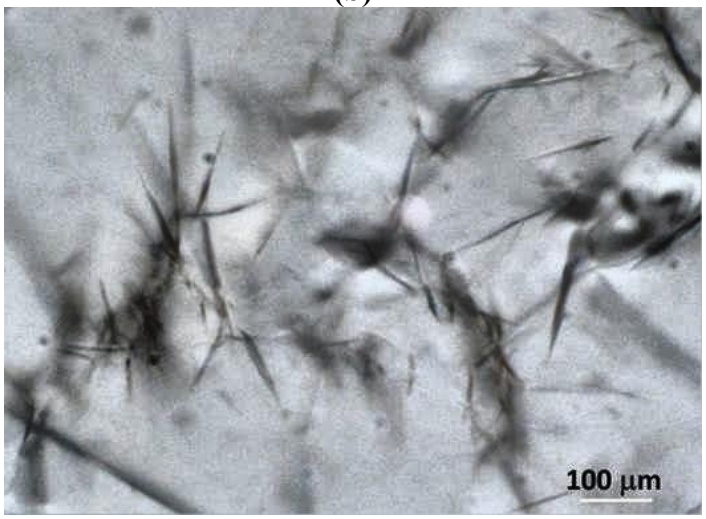

(c)